Nanoscale

Chiral Nematic Porous Germania and Germanium/Carbon Films

Journal:	*Nanoscale*
Manuscript ID:	NR-ART-04-2015-002520.R1
Article Type:	Paper
Date Submitted by the Author:	13-Jun-2015
Complete List of Authors:	Xu, Jing; National University of Defense Technology, College of Aerospace Science and Engineering Nguyen, Thanh-Dinh; UBC, Chemistry Xie, Kai; National University of Defence Technology, Department of Material Science and Applied Chemistry Hamad, Wadood; FPInnovations, CNC-Biomaterials Group; UBC, Chemistry MacLachlan, Mark; UBC Chemistry, Chemistry Department

Nanoscale

ARTICLE

Received xxxxxxxxxxxx,

Accepted xxxxxxxxxxxx

DOI: 10.1039/x0xx00000x

www.rsc.org/

Chiral Nematic Porous Germania and Germanium/Carbon Films

Jing Xu[a], Thanh-Dinh Nguyen[b], Kai Xie[a], Wadood Y. Hamad[c] and Mark J. MacLachlan†[b]

We report our extensive attempts and, ultimately, success to produce crack-free, chiral nematic GeO_2/cellulose nanocrystal (CNC) composite films with tunable photonic properties from the controlled assembly of germanium(IV) alkoxides with the lyotropic liquid-crystalline CNCs in a mixed solvent of water/DMF. With different pyrolysis conditions, the photonic GeO_2/CNC composites can be converted into freestanding chiral nematic films of amorphous GeO_2, and semiconducting mesoporous GeO_2/C and Ge/C replicas. These new materials are promising for chiral separation, enantioselective adsorption, catalysis, sensing, optoelectronics, and lithium ion batteries. Furthermore, the new, reproducible synthesis strategies developed may be applicable for constructing other composites and porous materials with chiral nematic ordering.

Introduction

Cellulose nanocrystals (CNCs) are a nanoscopic form of cellulose (~5-20 nm x 100-300 nm, depending on the preparation and cellulose source) obtained by acid-catalyzed hydrolysis of biomass.[1-5] CNCs form a chiral nematic liquid-crystalline (LC) phase in water that can be preserved in dried films.[6-12] In the solid films, the nanorods of CNCs are organized into layers whose orientation rotates through the stack with a characteristic pitch. In fact, the helicoidal structure in these films resembles the Bouligand-type structure observed for chitin in crab cuticles[13, 14] and the exoskeletons of many insects,[15] and the arrangement of cellulose in plant cell walls.[16, 17] In many examples, the Bouligand organization is responsible for the vivid iridescence that can be observed.[18]

CNCs are proving to be very useful materials for diverse applications.[19-24] Using CNCs dispersed in aqueous suspension as a LC template, our group recently constructed a family of photonic mesoporous materials with chiral nematic ordering.[25, 26] When CNCs are cast with silica or organosilica precursors, freestanding composite films of CNCs embedded in the inorganic matrix are obtained. Following removal of CNCs in the composites by either calcination or acid-catalyzed hydrolysis, film replicas of chiral nematic mesoporous silica,[27] organosilica,[28] and carbon[29] are obtained. These materials have pores about 3-10 nm in diameter that are organized into a layered, helicoidal arrangement. As the pitch of the helicoidal structure is on the order of the wavelengths of visible light, these films behave as photonic structures[30] and selectively reflect light of a given wavelength – they appear brilliantly iridescent. It is worth noting that the chiroptical properties of these photonic materials can be tuned by simply changing the length of the helical pitch. Therefore, these novel materials are attractive for chiral separation, optical devices, sensors, catalyst supports, and energy-storage materials[19, 26, 31, 32]

Although aqueous LC suspensions of CNCs were discovered over sixty years ago,[5] research on the LC properties of unfunctionalized CNCs in organic solvents has been very limited.[33] Recently our group[34] and Gray et al.[35] demonstrated that lyotropic chiral nematic LC phases can be formed by dispersing neutralized sulfated CNCs in polar organic media such as *N,N*-dimethylformamide (DMF). This new route successfully expanded the use of CNCs to template polymers with precursors that are incompatible with the aqueous CNC suspensions. We showed, for example, that highly hydrophobic polymers, such as polystyrene, can be co-assembled with CNCs in DMF to give iridescent composite films with chiral nematic order.[34]

Germanium, like silicon, is an important semiconductor and has attracted extensive interest in many areas such as optoelectronics, detectors, and solar cells.[36-39] Germanium oxide has a refractive index higher than that of silica,[40] which may improve the optical properties of the photonic structures. Extending the chiral nematic mesoporous frameworks to germanium-constituted materials may produce new types of multifunctional nanostructures that combine the optoelectronic properties of semiconductors with internal porosity and long-range chiral order. Such systems are also intriguing for optoelectronics, sensing, lithium ion batteries, and catalysis.[36-39, 41] One might anticipate that as germanium is silicon's neighbor on the periodic

[a]*Department of Material Science and Engineering, College of Aerospace Science and Engineering, National University of Defense Technology (NUDT), Changsha, Hunan 410073, P. R. China*

[b]*Department of Chemistry, University of British Columbia, 2036 Main Mall, Vancouver, British Columbia, V6T 1Z1, Canada*

[c]*FPInnovation, 2665 East Mall, Vancouver, British Columbia, V6T 1Z4, Canada*

Electronic Supplementary Information (ESI) available: [TGA, IR, Raman, TEM, SEM, BET]. See DOI: 10.1039/x0xx00000x

table, it would be straightforward to incorporate germanium into a photonic chiral structure. However, it is widely known that germanium(IV) species have considerably faster kinetics of hydrolysis and condensation than silicon(IV) analogues.[42, 43] As well, germania is more reactive than silica, which can lead to inhomogeneous nanostructured materials. Nonetheless, researchers succeeded in making ordered porous germania and other germanium-containing materials through several approaches such as LC templating, solvothermal synthesis, reverse micelles, and reduction.[44-57] Some of these materials show chiral nanostructured features organized in porous channels[45] or along helical chains,[50] but their chirality does not lead to photonic properties. To date, the synthesis of germanium-containing structures with chiral nematic organization at a larger length scale has not been reported. The chemical stability of germanium nanocrystals could be increased by combining with carbon supports into hybrid composites, which improves the electrical conductivity for the design of efficient lithium ion battery anode materials.[58, 59]

Here we present a new method to synthesize freestanding films of amorphous GeO_2 and mesoporous GeO_2/C and Ge/C with chiral nematic order by hydrolyzing germanium alkoxides during the self-assembly of the CNC dispersions in a mixed solvent system of water and DMF. These are the first germanium-based materials to present long-range chiral nematic order. It is also the first use of a mixed solvent system (in this case, water and DMF) to template materials with unfunctionalized CNCs. The reflectance peak of the chiral nematic solid films of CNCs and GeO_2/CNC composites cast from the CNC suspension can be tuned over a wide range of wavelengths by simply changing the proportion of water and DMF used. Furthermore, the new synthesis approaches developed here can provide effective strategies to produce other composites and porous materials, where the condensation of the precursor is incompatible with the self-assembly of CNCs in water (*e.g.*, TiO_2, SnO_2, Al_2O_3, or hydrophobic organosilica).

Results and Discussion

We first attempted to synthesize GeO_2/CNC composite films in water, but when the germanium alkoxide was added to the aqueous CNC dispersion, condensation products formed immediately and phase-separated from the CNCs. As a result, we obtained only cloudy, inhomogeneous films made of the assembly of slightly iridescent CNC layers on top of the particle aggregates of white germania. This was not surprising because the hydrolysis and condensation of germanium alkoxides are very fast in water.

Based on our previous experience with silica, it is crucial that the hydrolysis/condensation rate of the inorganic component is compatible with the self-assembly of CNCs. DMF is a well-known drying control chemical additive (DCCA) for sol-gel technology,[60] which could be used here to lower the high activity of germanium precursors and inhibit further condensation and agglomeration of germanium-containing species. To hydrolyze germanium precursors without disrupting the chiral nematic organization of CNCs, we added DMF to the aqueous CNC dispersion to reduce the effective concentration of water, thereby lowering the reactivity of germanium precursors. Visually, dispersions of CNCs in water/DMF with $Ge(OEt)_4$ remained homogeneous and dried at room temperature to form freestanding, crack-free GeO_2/CNC composite films (Figure 1). The composites appear transparent and strongly iridescent, demonstrating that the films are a homogeneous solid phase. We found that the films cast from the CNC suspension in water/DMF greatly improve the cracking and brittleness possibly due to the reduced hydrogen bonding between CNCs and slower evaporation of the water. Thus, the largest samples of crack-free composite films we prepared are about 6 cm in diameter and about 30 μm in thickness, but there is no apparent limitation to the size.

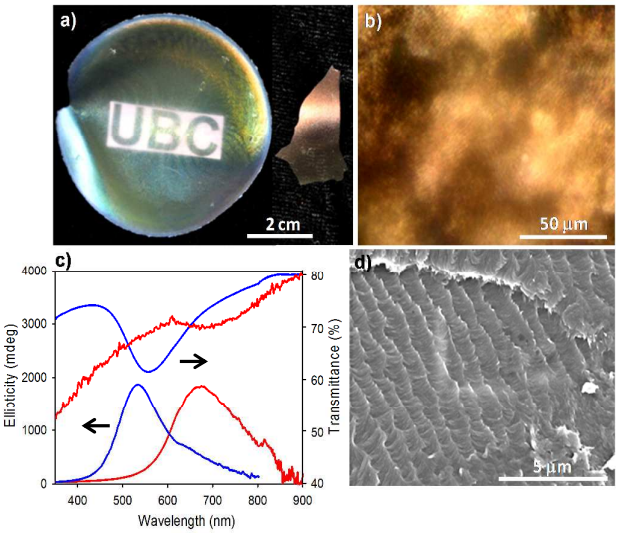

Figure 1. Chiral nematic germania/CNC composite films. (a) Photograph of GeO_2/CNC composites cast from the evaporation of $Ge(OEt)_4$/CNC suspensions with variable water/DMF ratio of 1:2 (left) and 1:1 (right) under ambient conditions. Note that the blue film (left) kept its original shape after air-drying, while the red film (right) was manually broken into smaller sized pieces. (b) POM image of the GeO_2/CNC composites. (c) UV-vis transmittance spectra (right) and CD spectra (left) of these two GeO_2/CNC composites obtained from the CNC suspensions with water/DMF ratio of 1:2 (blue trace) and 1:1 (red trace). Increasing the proportion of DMF in the mixed aqueous suspension results in a blue shift in the reflectance peaks of the films. (d) SEM image of fracture cross-sections of the GeO_2/CNC composite film revealing a left-handed chiral nematic structure with pitch distance to be of the order of several hundred nanometers.

Both the addition of DMF and controlling the ratio of DMF to water are very important for the successful synthesis of GeO_2/CNC composite films with chiral nematic order. We found that controlling the ratio of water/DMF and the proportion of germanium precursors relative to CNCs in the dispersion during self-assembly allow for tuning the structural coloration in the GeO_2/CNC composites (Figure 1). The composite films show a change in iridescence from yellow-red to yellow-green when the volume fraction of DMF added was increased from 30 to 70 vol% in water, or when the germanium precursor was decreased from 70 to 30 wt% (relative to CNCs). Polarized optical microscopy (POM)

images of the composite films show fingerprint textures characteristic of a chiral nematic structure with strong birefringence (Figure 1b). Optical spectroscopy shows the tunability of the chiroptical properties of the composites by varying their helical pitch (Figure 1c). The composites with germanium alkoxide loading of 62 wt% used in the preparation show a reflectance peak that can be tuned from ~550 nm to ~680 nm by simply changing the water/DMF ratio from 1:2 to 1:1. Circular dichroism (CD) spectra of these same samples show an intense signal with positive ellipticity at the same wavelength as the reflectance peak. The CD spectra show no significant change as the sample is rotated, indicating that the signal is not dominated by linear birefringence (Figure S2). The peak reflected wavelength observed by UV-vis spectroscopy matches well with the position of the positive CD peak, demonstrating that the left-handed chiral nematic order was preserved in the GeO_2/CNC composites and the structural coloration derives from the selective reflection of left-handed circularly polarized light. This tuning of the iridescence may originate from DMF in the aqueous dispersion reducing the effective ionic strength of CNCs. We also clearly observed this optical effect in iridescent CNC films that were prepared by using the same method, but without loading $Ge(OEt)_4$.

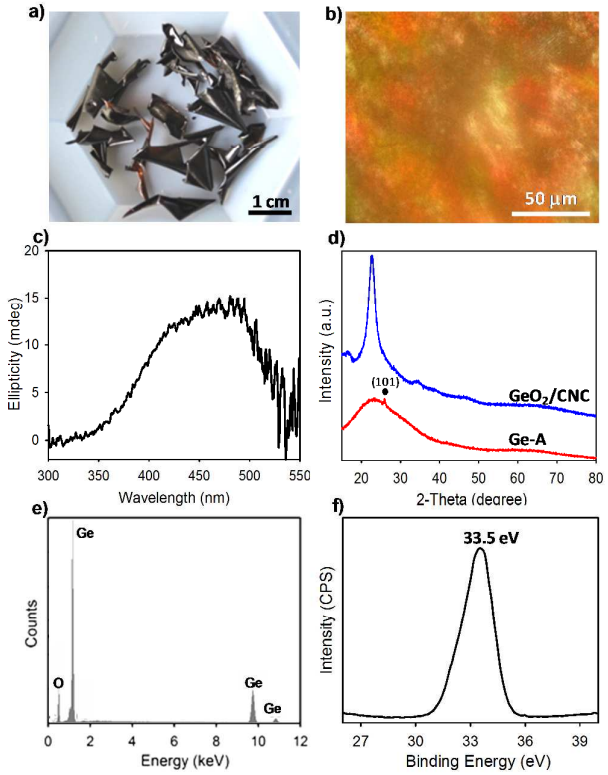

Figure 2. Chiral nematic amorphous germania films (**Ge-A**). (a) Photograph, (b) POM image, (c) CD spectrum of **Ge-A**. (d) PXRD patterns of GeO_2/CNC composites (blue line) and **Ge-A** (red line). (e) EDX spectrum and (f) High-resolution Ge 3d XPS spectrum of **Ge-A**.

Also, some change in the peak reflected wavelength was observed when the proportion of germanium alkoxide relative to CNCs was varied. This change is related to the tuning of the pitch of the CNC template by varying the amount of germanium precursor loaded in the composite. However, this chiroptical tunability was not as sensitive to changes as the proportion of silica precursor employed in silica/CNC composite films,[27] where the peak wavelength reflected is drastically changed by varying the proportion of tetraalkoxysilane and CNCs. The reason for the diminished effect in the case of germania might be caused by both the different charge densities on the germanium alkoxide hydrolysis intermediates and the DMF solvent screening the charges on the resultant inorganic phase and on the surface of the CNCs.

The GeO_2/CNC composite films were analyzed by scanning electron microscopy (SEM). An apparent layered structure with repeating distance of several hundred nanometers can be observed along the fracture cross-sections of the composites (Figure 1d, S3). This distance is consistent with the observation of the reflection in the visible range of the spectrum. The SEM images also reveal a twisting spindle-like morphology that rotates in a counter-clockwise direction over micrometer distances characteristic of a left-handed twisted structure. This structure is very similar to the chiral nematic organization present in pure CNC films prepared from drying aqueous dispersions.[61] The addition of DMF allowed us to tame the high reactivity of the germanium precursor in the lyotropic LC phase and obtain relatively homogeneous composite films that retain the long-range chiral nematic order of CNCs.

We tried to synthesize the composite films in pure DMF by using the CNC dispersion in DMF prepared from our previously reported method.[34] In fact, iridescent germanium-containing composites with chiral nematic ordering can be obtained easily, but the pyrolyzed samples were fragile and we were unable to remove the CNC template by calcination without substantial loss of chirality and structure in the films. We believe that the small amount of residual water present in DMF leads to a low degree of the hydrolysis and condensation of germanium alkoxide in DMF. Without a sufficiently robust interconnected network within the composite, the structure collapses during the removal of CNCs by combustion. Also, unhydrolyzed germanium species are relatively volatile and may evaporate during either self-assembly of the films or calcination, causing a large shrinkage of the films and subsequent collapse of the templated structure. Thus, it is necessary to use a mixed solvent system, and by employing a mixture of DMF and water, we can produce tunable photonic chiral nematic GeO_2/CNC composite films with a wide range of composition (~0-30 wt% germania). This new route is highly reproducible to yield large, uniform photonic GeO_2/CNC composite films.

As the next step, we used the chiral nematic GeO_2/CNC composites with a high degree of order and tunable chiroptical properties as novel precursors for the production of secondary germanium-based nanostructured replicas. Starting from the chiral nematic GeO_2/CNC composites already described, we can obtain three types of the porous germanium-based thin films with chiral nematic structures by varying different pyrolysis conditions: GeO_2 (denoted as **Ge-A**), GeO_2/C (denoted as **Ge-N**), and Ge/C (denoted as **Ge-H**) were produced by calcining the GeO_2/CNC composites under air at 500 °C, under N_2 at 600 °C, and 10% H_2/90% N_2 at 700 °C, respectively (additional details in Experimental Section).

Calcination of the GeO_2/CNC composites under air afforded freestanding films (**Ge-A**) that appear a little curled but they mostly retain the overall shape of the original composites with dimensions of several centimeters. The calcined products are glossy brown, brittle films with slight transparency (Figure 2a). IR bands associated with vibration modes of CNCs (*i.e.*, CH_2 scissoring motion at 1430 cm^{-1}, C–O–C pyranose ring stretching vibration at 1050 cm^{-1}) are absent in the calcined films after cellulose removal, but a strong germanol band is present at 870 cm^{-1} (Figure S4).[62, 63] Elemental analysis (EA) shows a small amount (1.5-6 wt%) of residual carbon in **Ge-A**, in good agreement with energy-dispersive X-ray (EDX) analysis (Figure 2e). Powder X-ray diffraction (PXRD) patterns (Figure 2d) show that the GeO_2/CNC composites have diffraction peaks characteristic of the cellulose nanocrystals, while the calcined samples obtained after cellulose removal have a broad hump at 23° 2θ characteristic of amorphous germania[64] and a weak, sharp peak at 25.9° 2θ attributed to the generation of a small amount of crystalline hexagonal germania.[58] This indicates that germania in **Ge-A** is mainly amorphous. It is interesting to point out that the amorphous GeO_2 thin films were still obtained even after calcination at high temperature. A high-resolution Ge 3d XPS spectrum (Figure 2f) of **Ge-A** shows a strong main peak at 33.5 eV attributed to Ge^{4+}, which indicates the formation of germanium dioxide in the **Ge-A** film.[58] These results are fully consistent with the removal of the CNC template in the composites to yield GeO_2 films.

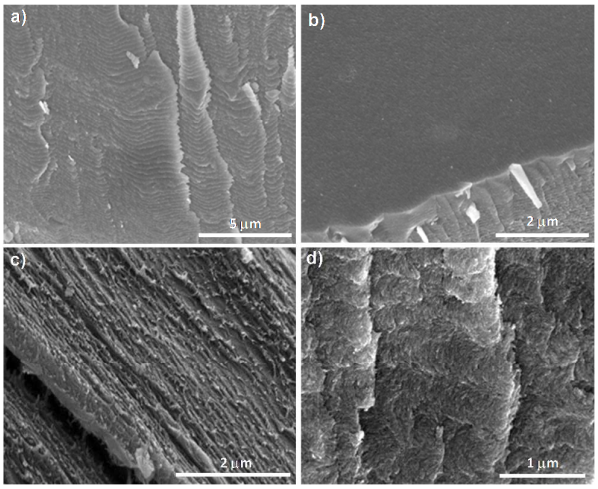

Figure 3. SEM images of germanium-containing materials with chiral nematic organization. **Ge-A** viewed along fracture cross-sections (a) showing stacked layers resulting from the helical pitch of the chiral nematic phase and viewed at the top of the film surfaces (b) revealing the relatively smooth top surface and layered structure looking down the edge. (c) Cutting edge view of **Ge-N**. (d) Cross sectional view of **Ge-H** showing a twisting, layered structure.

Since conventional germanium dioxide powder is white, most of the dark brown color of the resulting GeO_2 films is thought to result from black carbon residues in the materials. It is also possible that some GeO or even metallic Ge could be generated through the reduction of GeO_2 with carbon formed during the pyrolysis of the CNC template (as $GeO_2 + C \rightarrow GeO + CO_2$; $GeO_2 + C \rightarrow Ge + CO_2$).[58] Trace amounts of brown GeO[65] and dark-brown metallic germanium[66] may contribute to enhance the dark brown color in the GeO_2 films, although we did not obtain evidence for these contaminants from the PXRD or XPS analyses of the **Ge-A** samples.

The strong birefringence and fingerprint textures of the GeO_2 films (**Ge-A**) that can be observed when the films are viewed under crossed polarizers are characteristic of the chiral nematic features (Figure 2b). Due to the low transparency and dark brown color of the films, the chiroptical properties of the materials could not be characterized by UV-vis transmission spectroscopy. However, we observed a weak positive CD signal at ~480 nm (Figure 2c) that may provide evidence for the left-handed chiral structure existing in **Ge-A**, although the intensity of the CD signal is not as strong as those observed for the GeO_2/CNC composites. From SEM images of **Ge-A** (Figure 3a,b), we can observe an apparent twisting layered structure of the spindle-like features perpendicular to the top surfaces of the films, which confirms the retention of the chiral nematic organization in the GeO_2 structure. These spindle-like nanostructured features organized with long-range ordered alignment, as observed by viewing the flat top surface of the films, resemble those observed from chiral nematic mesoporous silica[27] and titania[67] structures. Compared to the latter, the surfaces of the amorphous GeO_2 films are smoother and more homogeneous without a rough "crust" coating (Figure S6). The rough "crust" coating usually found on the surfaces of the mesoporous titania crystal films result from the partial condensation of TiO_2 precursors on the surfaces of the mesoporous silica template.[67] This reveals another advantage of our co-assembly method: as compared to the usual hard-templating method, the co-assembly process leads to highly homogenous structures since all of the components of the assembled materials are evenly dispersed in solution at the molecular level.

Nitrogen adsorption was carried out on the **Ge-A** samples to study their porosity (Figure S7). However, BET (Brunauer-Emmett-Teller) surface areas of **Ge-A** samples are very low, ranging from only 10 to 40 $m^2 g^{-1}$. We tried many different synthetic conditions to obtain mesoporous germania by calcining the GeO_2/CNC composites under air, but the resulting materials showed low porosity in every case. Taken together, we can conclude that the GeO_2 films have faithfully replicated the chiral nematic order of the CNC template, but in the process of removing CNCs the amorphous GeO_2 structures shrunk substantially, leading to blocking of any pores.

We prepared films of **Ge-N** and **Ge-H** by calcining the GeO_2/CNC composites under flowing pure N_2 and 10% H_2/90% N_2, respectively. Both the resulting films with dimensions of several centimeters are black with a metallic sheen and some samples appear iridescent (Figures 4a, 5a), and **Ge-N** is darker than **Ge-H**. These materials are less brittle than the GeO_2 films, indicating that the mechanical strength of these thin films is enhanced by combining germania with carbon. EDX analyses (Figures 4c, 5c) confirm that **Ge-H** contains 79 wt% carbon, 18 wt% germanium, and 3.0 wt% oxygen, while **Ge-N** contains 66.5 wt% carbon, 20.9 wt% germanium, and 12.3 wt% oxygen. Thermogravimetric analysis (TGA) and EA show that **Ge-N** and **Ge-H** have similar carbon content

(Figure S5b,c). It appears that the pyrolysis of the GeO_2/CNC composites under pure N_2 and H_2/N_2 afforded carbon with nearly the same yield (approximately 30%). **Ge-H** has lower oxygen content than **Ge-N** owing to reduction by hydrogen from 10% H_2/90% N_2 compared to pure N_2.

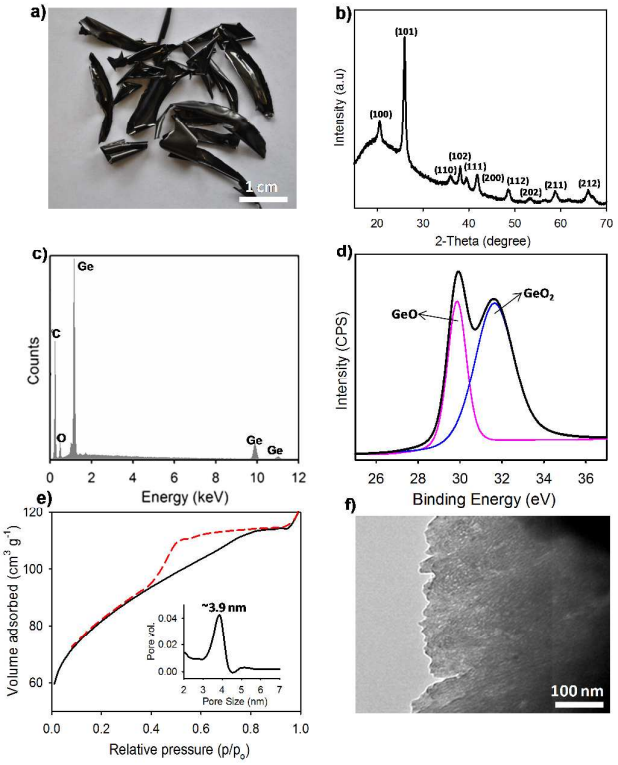

Figure 4. Chiral nematic mesoporous GeO_2/C composite films (**Ge-N**). (a) Photograph, (b) PXRD pattern, (c) EDX spectrum, (d) High-resolution XPS spectrum of Ge 3d region, (e) Nitrogen sorption isotherm; inset of BJH pore size distribution, and (f) TEM image of **Ge-N**.

We undertook PXRD, XPS, IR, and Raman spectroscopy studies of both **Ge-N** and **Ge-H** to probe the structural properties of these new materials. The PXRD pattern of **Ge-N** shows diffraction peaks as marked in Figure 4b, indexed to hexagonal germania[58] in the absence of a metallic germanium phase. Unlike the amorphous GeO_2 films (**Ge-A** obtained at 500 °C), higher temperature (600 °C) of calcination for **Ge-N** led to crystallization of GeO_2 in the composites. However, the PXRD pattern (Figure 5b) of **Ge-H** shows intense sharp reflections at 27.5°, 45.6°, 53.5°, 66.4° 2θ indexed to a pure diamond lattice metallic germanium[66] and no hexagonal germania phase is observed. The diffractograms of both these materials also show a broad hump at 23° 2θ characteristic of amorphous carbon.[29] Both **Ge-N** and **Ge-H** have amorphous carbon derived from CNCs under pyrolysis and this was further confirmed by Raman spectroscopy (Figure S8), which shows broad D and G bands at 1320 and 1595 cm^{-1}, respectively.[29] IR spectra (Figure S4) of **Ge-N** show an intense band at 870 cm^{-1} assigned to the symmetric Ge–O–Ge anti-symmetric stretching mode,[68] while the absence of this band in **Ge-H** further suggests the complete reduction of GeO_2 to Ge by hydrogen in **Ge-H**. A high-resolution Ge 3d XPS spectrum (Figure 5d) of **Ge-H** shows a strong main peak at 29.0 eV attributed to Ge(0),[69] which thus provides strong evidence that Ge was indeed reduced to zero-valent Ge from the original, oxidized starting material GeO_2/CNC. In contrast, a high-resolution Ge 3d XPS spectrum of **Ge-N** (Figure 4d) shows two peaks at 29.9 eV and 31.8 eV attributed to GeO and GeO_2, respectively.[70] The data indicate that most of GeO_2 was generated in **Ge-N** during calcination under N_2 in accordance with the PXRD results and the formation of some GeO may be caused by reducing GeO_2 by carbon. These results confirm that the GeO_2/CNC composites were converted to the hexagonal GeO_2/C under pure N_2, and to the diamond Ge/C under H_2/N_2 by a complete reduction of Ge^{4+} to Ge^0 during calcination.

The porosity of **Ge-N** and **Ge-H** was studied by N_2 sorption isotherms (Figures 4e, 5e). A typical type-IV isotherm with type-H2 hysteresis was observed for both these samples, which indicates an introduction of mesoporosity into the composite materials. *t*-Plot analyses show that **Ge-N** and **Ge-H** are predominately mesoporous with very little microporosity. This is consistent with pores arising from the carbonization of the CNC templates, which are several nanometers in diameter and would be expected to yield mesopores in the host when they are removed or completely converted into carbon. The BET surface area was found to be ~269 $m^2 g^{-1}$ for **Ge-N** and ~254 $m^2 g^{-1}$ for **Ge-H** with corresponding pore volume of ~0.19 $cm^3 g^{-1}$ and ~0.18 $cm^3 g^{-1}$. The pore diameter of **Ge-N** is about 3.6 nm, which is slightly smaller than that of **Ge-H** (~3.9 nm) (inset of Figures 4e, 5e). TEM images of **Ge-N** (Figures 4f, S9) show long-range aligned pores corresponding well to the chiral nematic organization, which confirms the mesoporous structures of the carbonized composite films. These TEM results resemble those previously observed for chiral nematic mesoporous carbon.[29]

It should be noted here that the mesopores of **Ge-N** and **Ge-H** arise in the presence of the germanium species, which is likely different from the chiral nematic mesoporous carbon derived from the silica/CNC composites. For the latter, the mesoporosity resulted from the spaces where silica occupied and mesopores are expected to occur only after the silica component was removed from the silica/carbon composites. In GeO_2/C and Ge/C, the mesoporosity arises with the germanium species still in the films. These results suggest that during carbonization of CNCs in the composites, the combustion of cellulose yields the mesopores within the germanium matrix.

SEM measurements were performed on both **Ge-N** and **Ge-H** (Figure 3c,d). From the SEM images perpendicular to the top surfaces of the films, we see twisting layered structures with long-range ordering that are similar to the chiral nematic structures observed in the GeO_2/CNC composites and the pure CNC films. The repeating distance (*i.e.*, pitch) in **Ge-N** and **Ge-H** appears shorter than that of the GeO_2/CNC composites. The decrease of the repeating distance is due to the shrinkage that occurs in the films during calcination or reduction, which also induces the blue shift of the peak wavelength reflected by the chiral nematic structure. Thus, only some samples of **Ge-H** obtained from the GeO_2/CNC composite prepared using the water/DMF ratio of 1:1 show iridescence in the visible region while the other samples have too

short of a helical pitch to reflect visible light. Also, because of their opaque, black color, we could not investigate the samples of **Ge-N** or **Ge-H** by POM and CD techniques. But the SEM images present direct evidence for the retention of the chiral nematic structure in both the mesoporous GeO_2/C and Ge/C films.

Germanium-based materials are intriguing anode materials in high capacity lithium-ion batteries (LIBs).[41, 58, 59, 71-73] So far, poor cycling stability is one of the main obstacles for application of the germanium-based materials in LIBs. Introducing mesoporosity into the Ge/C structure may enhance the cycling performance of LIBs because the continuous network can provide efficient electronic pathway for Ge.[74] Also, the mesoporous structures could buffer the pulverization and delamination of the Ge electrodes that result from a large volume change (~200%) during the alloying reaction of the active material with lithium.[75] In terms of this aspect, the chiral nematic amorphous GeO_2 films could be a novel precursor for reduction to porous Ge semiconductor replicas useful for LIBs.[57]

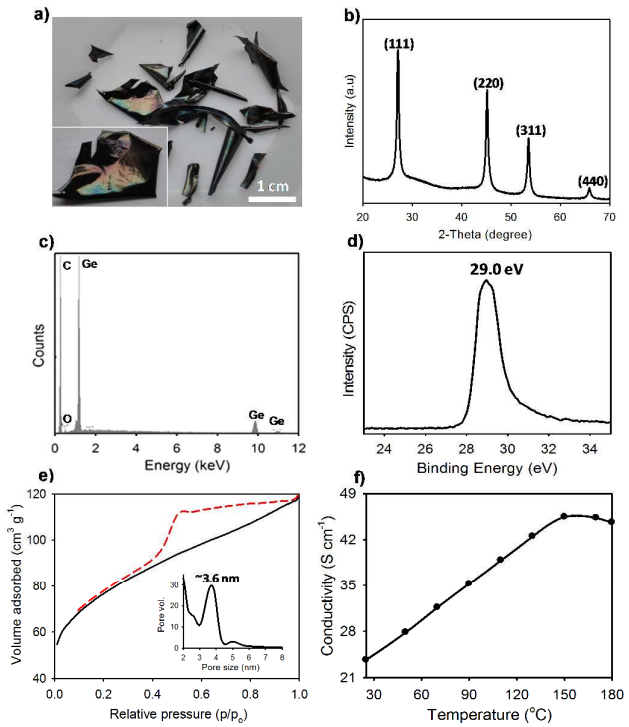

Figure 5. Chiral nematic mesoporous Ge/C composite films (**Ge-H**). (a) Photograph, (b) PXRD pattern, (c) EDX spectrum, (d) Ge 3d XPS spectrum, (e) Nitrogen sorption isotherm; inset of BJH pore size distribution, and (f) Temperature-dependent conductivity plot of **Ge-H**.

The temperature-dependent conductivity of the carbonized GeO_2/CNC composites was investigated using a four-probe method. Figure 5f shows that the conductivity of the Ge/C films (**Ge-H**) increases from 24 to 46 S cm^{-1} between 25 °C and 150 °C, indicating semiconducting behavior. Compared to pure crystalline Ge with a conductivity of around 2.13×10^{-2} S cm^{-1} at 27 °C,[76] the conductivity of **Ge-H** is increased significantly by the introduction of a mesoporous network into the Ge/C composite. The good conductivity of **Ge-H** is beneficial for enhancing both the cycling stability and the rate capability of LIBs. Furthermore, **Ge-H** has the advantage that it is readily obtained as a freestanding film with centimeter dimensions, thereby eliminating the need for a binder, which is usually necessary for other electrode materials. Like Ge/C, GeO_2/C was also previously studied as an anode material for highly reversible LIBs.[72, 77]

Conclusions

We have shown, for the first time, that freestanding porous germanium-based thin films with long-range chiral nematic order were synthesized by direct co-assembly of germanium(IV) alkoxides with CNCs in a mixed solvent system of water/DMF. Both the high surface area and chiral nematic organization of the CNC template were cast in the GeO_2/CNC composites. Starting from these new photonic composite films, different colorful materials such as amorphous GeO_2, and mesoporous GeO_2/C and Ge/C structures with chiral nematic order were obtained through simple changes in pyrolysis conditions. These novel materials may be useful for separation, adsorption, catalysis, sensing, optoelectronics, and lithium ion batteries. We also found that the mixed water/DMF solvents allow for good control of the simultaneous hydrolysis of metal alkoxides and CNC assembly. We are investigating the lithium ion storage properties of the mesoporous Ge/C and GeO_2/C composites and investigating the extension of the mixed solvent assembly to construct other materials with chiral nematic ordering.

Acknowledgements

This work was supported by the Natural Sciences and Engineering Research Council (NSERC) of Canada. JX thanks the National University of Defense Technology (NUDT), China for supporting her stay as a visiting professor at UBC. TDN thanks NSERC for a postdoctoral fellowship. We are grateful to CelluForce Inc. for donating CNCs for this research.

Experimental Section

Preparation of CNCs

Aqueous suspensions of CNCs were provided by CelluForce Inc., and were prepared according to a literature procedure[9] by controlled sulfuric acid hydrolysis of commercial bleached kraft softwood pulp. Hydrolysis was carried out with 64% (w/w) sulfuric acid at 45 °C for 25 min with constant stirring (8.75 mL of a sulfuric acid solution/g pulp). Immediately following the acid hydrolysis, the suspension was diluted 10-fold with cold deionized water to quench the reaction and allowed to settle overnight. The clear top layer was decanted and the remaining white cloudy layer was centrifuged at 4000 rpm for 10 min. The resultant precipitate was rinsed 2 times and dialyzed against deionized water until constant pH (~ 6) for 5 d. After dialysis, the suspension was dispersed by subjecting it to ultrasound treatment using a Fisher Sonic Dismembrator for 30 min at 60% output and finally filtered with Whatman No. 42 filter paper. The final concentration of the resultant aqueous suspension was

approximately 2% (w/w), and the pH and concentration adjusted as desired. Sulfuric acid hydrolysis yielded CNC containing negatively charged surface sulfate groups (~5.2 per 100 glucose monomers). The physical dimensions of spindle-shaped cellulose nanocrystals were measured, via TEM, to be 15 ± 8 nm by 195 ± 93 nm with an aspect ratio of ~13 (Figure S1). The crystallinity index of cellulose nanocrystals was determined to be 92% on the basis of PXRD, followed by deconvolution of the patterns using the Ruland-Rietveld method.[9]

Preparation of chiral nematic GeO_2/CNC composites

Aqueous suspensions of CNCs (4.24 wt%, pH 2.4) were used for the preparation of GeO_2/CNC composites. Germanium precursors of tetraisopropoxygermane (TPOG) or tetraethoxygermane (TEOG) were used for these syntheses. In a typical procedure, 0.10 mL TPOG in 6 mL DMF was added to 2 mL the aqueous CNC suspension. The mixture was stirred for 10 min and poured into a 60 mm diameter polystyrene Petri dish. After slow evaporation under ambient conditions within 48 h, freestanding GeO_2/CNC composite films (100 mg) were obtained. To prepare the composite films with tunable photonic properties, additional samples were prepared by using an identical procedure except for varying the amount of either DMF or germanium precursor incorporated.

Preparation of chiral nematic porous films of GeO_2, GeO_2/C, and Ge/C materials

The removal of the cellulose template in the GeO_2/CNC composites (300 mg) was accomplished by heating the samples under flowing air to 100 °C at 2 °C min^{-1}, holding at 100 °C for 2 h, then heating to 500 °C at 2 °C min^{-1} and holding at 500 °C for 4 h. Freestanding GeO_2 films (**Ge-A**) (110 mg) were obtained after cooling the samples to room temperature. Mesoporous GeO_2/C composites (**Ge-N**), (140 mg) were prepared by heating the GeO_2/CNC composites (300 mg) under flowing N_2 at a rate of 2 °C min^{-1} to 100 °C, holding at 100 °C for 2 h, then heating to 600 °C for 6 h. Mesoporous Ge/C composites (**Ge-H**) (130 mg) were prepared by heating the GeO_2/CNC composites (300 mg) under 10%H_2/90%N_2 at 2 °C min^{-1} to 100 °C, holding at 100 °C for 2 h, then heating to 700 °C at 2 °C min^{-1}, and holding at 700 °C for 6 h. Note that the GeO_2/CNC composites with the water/DMF ratio of 1:2 were used to prepare GeO_2 (**Ge-A**) and GeO_2/C (**Ge-N**), while Ge/C (**Ge-H**) was prepared from the GeO_2/CNC composites with the water/DMF ratio of 1:1.

Structural Characterization

Ultraviolet-visible/near-infrared spectra were measured using a Cary 5000 UV-Vis/NIR spectrophotometer. Polarized optical microscopy was collected on an Olympus BX41 microscope. Thermogravimetric analysis was conducted on a PerkinElmer Pyris 6 thermogravimetric analyzer. Infrared spectroscopy was obtained by using a Nicolet 6700 FTIR spectrometer equipped with a Smart orbit diamond attenuated total reflectance (ATR) attachment. Power X-ray diffraction patterns were collected on a D8 advance X-ray diffractometer. TEM images were collected on a Hitachi H7600 electron microscope. In terms of sample preparation, samples were ground into small pieces, dispersed in ethanol, then dropcast onto a copper TEM grid, allowing the solvent to evaporate under ambient conditions. SEM images were obtained by using a Hitachi S4700 electron microscope after sputter-coating the samples with either Au or Au-Pd. Energy-dispersive X-ray (EDX) analysis was collected using a Hitachi S2300 scanning electron microscope. Gas adsorption experiments were conducted on a Micromeretics Accelerated Surface Area & Porosity (ASAP) 2020 system. CD spectroscopy was measured using a JASCO J-710 spectropolarimeter. The standard four-probe method was used to investigate the electrical conductivity of the mesoporous films. The voltage and current were measured by using Hewlett–Packard model 34401A and 3478A multimeters, respectively. To collect the temperature-dependence of the electrical conductivity, the temperature of the film was varied over a range of 20 °C to 180 °C using a temperature-controlled heater. Raman spectroscopy was performed using a SpectraCode model RP-1 spectrometer with a 785 nm diode laser excitation. XPS measurements were obtained in an ion-pumped chamber (evacuated to 10^{-9} Torr) of a photoelectron spectrometer (Leybold MAX200) equipped with a focused Al K_α X-ray source.

Notes and references

1. Y. Habibi, L. A. Lucia, O. J. Rojas, *Chem. Rev.* 2010, *110*, 3479-3500.
2. D. Klemm, D. F. Kramer, S. Moritz, T. Lindstrom, M. Ankerfors, D. Gray, A. Dorris, *Angew. Chem. Int. Ed.* 2011, *50*, 5438-5466.
3. M. Mariano, N. E. Kissi, A. Dufresne, *J. Poly. Sci. B* 2014, *52*, 791-806.
4. M. A. S. A. Samir, F. Alloin, A. Dufresne, *Biomacromolecules* 2005, *6*, 612-626.
5. S. M. Mukherjee, H. J. Woods, *Biochim. Biophys. Acta*, 1953, *10*, 499-511.
6. R. H. Marchessault, F. F. Morehead, N. M. Walter, *Nature* 1959, *184*, 632-633.
7. J. F. Revol, H. Bradford, J. Giasson, R. H. Marchessault, D. G. Gray, *Int. J. Biol. Macromol*. 1992, *14*, 170-172.
8. X. Mu, D. G. Gray, *Langmuir* 2014, *30*, 9256-9260.
9. W. Y. Hamad, T. Q. Hu, *Can. J. Chem. Eng.* 2010, *88*, 392-402.
10. J. Majoinen, E. Kontturi, O. Ikkala, D. G. Gray, *Cellulose* 2012, *19*, 1599-1605.
11. C. Edgar, D. Gray, *Cellulose* 2001, *8*, 5-12.
12. S. Beck, J. Bouchard, G. Chauve, R. Berry, *Cellulose* 2013, *20*, 1401-1411.
13. Y. Bouligand, *Tissue Cell* 1972, *4*, 189-217.
14. T. D. Nguyen, M. J. MacLachlan, *Adv. Optical Mater.* 2014, *2*, 1031-1037.
15. V. Sharma, M. Crne, J. O. Park, M. Srinivasarao, *Science* 2009, *325*, 449-451.
16. S. Vignolini, P. J. Rudall, A. V. Rowland, A. Reed, E. Moyroud, R. B. Faden, J. J. Baumberg, B. J. Glover, U. Steiner, *Proc. Natl. Acad. Sci. USA* 2012, *109*, 15712-15715.
17. A. G. Dumanli, G. Kamita, J. Landman, J. Kooij, B. J. Glover, J. J. Baumberg, U. Steiner, S. Vignolini, *Adv. Optical Mater.* 2014, *2*, 646-650.
18. J. Sun, B. Bhushan, J. Tong, *RSC Advances* 2013, *3*, 14862-14889.

19. J. P. F. Lagerwall, C. Schutz, M. Salajkova, J. H. Noh, J. H. Park, G. Scalia and L. Bergstrom, *NPG Asia Mater*. 2014, *6*, e80.
20. R. M. A. Domingues, M. E. Gomes, R. L. Reis, *Biomacromolecules* 2014, *15*, 2327-2346.
21. Y. Nakai, M. Yoshikawa, *Polym. J.* 2014, 1-6.
22. K. Nagashima, H. Koga, U. Celano, F. Zhuge, M. Kanai, S. Rahong, G. Meng, Y. He, J. D. Boeck, M. Jurczak, W. Vandervorst, T. Kitaoka, M. Nogi, T. Yanagida, *Sci. Rep.* 2014, *4*, 5532.
23. R. T. Olsson, M. A. S. A. Samir, G. S. Alvarez, L. Belova, V. Strom, L. A. Berglund, O. Ikkala, J. Nogues, U. W. Gedde, *Nat. Nanotech.* 2010, *5*, 584-588.
24. H. Shafiee, W. Asghar, F. Inci, M. Yuksekkaya, M. Jahangir, M. H. Zhang, N. G. Durmus, U. A. Gurkan, D. R. Kuritzkes, U. Demirci, *Sci. Rep.* 2015, *5*, 8719.
25. J. A. Kelly, M. Giese, K. E. Shopsowitz, W. Y. Hamad, M. J. MacLachlan, *Acc. Chem. Res.* 2014, *47*, 1088-1096.
26. M. Giese, L. K. Blusch, M. K. Khan, M. J. MacLachlan, *Angew. Chem. Int. Ed.* 2015, *54*, 2888-2910.
27. K. E. Shopsowitz, H. Qi, W. Y. Hamad, M. J. MacLachlan, *Nature* 2010, *468*, 422-425.
28. K. E. Shopsowitz, W. Y. Hamad, M. J. MacLachlan, *J. Am. Chem. Soc.* 2012, *134*, 867-870.
29. K. E. Shopsowitz, W. Y. Hamad, M. J. MacLachlan, *Angew. Chem. Int. Ed.* 2011, *50*, 10991-10995.
30. J. F. G. Lopez, M. Ibisate, R. Sapienza, L. S. F. Perez, A. Blanco, C. Lopez, *Adv. Mater.* 2011, *23*, 30-69.
31. J. H. Zhang, S. M. Xie, M. Zhang, M. Zi, P. G. He, L. M. Yuan, *Anal. Chem.* 2014, *86*, 9595-9602.
32. B. Wang, X. Li, B. Luo, J. Yang, X. Wang, Q. Song, S. Chen, L. Zhi, *Small* 2013, *9*, 2399-2404.
33. S. E. Hafraoui, J. L. Putaux, L. Heux, *J. Phys. Chem. B* 2009, *113*, 11069-11075.
34. C. C. Y. Cheung, M. Giese, J. A. Kelly, W. Y. Hamad, M. J. MacLachlan, *ACS Macro Lett.* 2013, *2*, 1016-1020.
35. D. Viet, S. B. Candanedo, D. Gray, *Cellulose* **2007**, *14*, 109-113.
36. D. D. V. Li, R. E. Schaak, *Chem. Soc. Rev.* 2013, *42*, 2861-2879.
37. X. Wu, J. S. Kulkarni, G. Collins, N. Petkov, D. Almecija, J. J. Boland, D. Erts, J. D. Holmes, *Chem. Mater.* 2008, *20*, 5954-5967.
38. J. A. Kelly, E. J. Henderson, J. G. C. Veinot, *Chem. Commun.* 2010, *46*, 8704-8718.
39. C. Boztug, J. R. S. Perez, F. Cavallo, M. G. Lagally, R. Paiella, *ACS Nano* 2014, *8*, 3136-3151.
40. A. Margaryan, W. M. Liu, *Opt. Eng.* 1993, *32*, 1995-1996.
41. G. H. Lee, S. J. Kwon, K. S. Park, J. G. Kang, J. G. Park, S. Lee, J. C. Kim, H. W. Shim, D. W. Kim, *Sci. Rep.* 2014, *4*, 6883.
42. V. Krishnan, S. Gross, S. Müller, L. Armelao, E. Tondello, H. Bertagnolli, *J. Phys. Chem. B* 2007, *111*, 7501-7518.
43. V. Stanic, A. C. Pierre, T. H. Etsell, *J. Phys. Chem. A* 2001, *105*, 6136-6143.
44. G. S. Armatas, M. G. Kanatzidis, *Science* 2006, *313*, 817-820.
45. G. S. Armatas, M. G. Kanatzidis, *Nature* 2006, *441*, 1122-1125.
46. X. Zou, T. Conradsson, M. Klingstedt, M. S. Dadachov, M. O'Keeffe, *Nature* 2005, *437*, 716-719.
47. D. Sun, A. E. Riley, A. J. Cadby, E. K. Richman, S. D. Korlann, S. H. Tolbert, *Nature* 2006, *441*, 1126-1130.
48. G. S. Armatas, M. G. Kanatzidis, *J. Am. Chem. Soc.* 2008, *130*, 11430-11436.
49. X. Meng, R. A. Salman, J. Zhao, N. Borissenko, Y. Li, F. Endres, *Angew. Chem. Int. Ed.* 2009, *48*, 2703-2707.
50. M. L. Feng, D.-N. Kong, Z. L. Xie, X. Y. Huang, *Angew. Chem. Int. Ed.* 2008, *47*, 8623-8626.
51. L. K. Vugt, A. F. Driel, R. W. Tjerkstra, L. Bechger, W. L. Vos, D. Vanmaekelbergh, J. J, Kelly, *Chem. Comm.* 2002, 2054-2055.
52. Y. M. Lin, K. C. Klavetter, A. Heller, C. B. Mullins, *J. Phys. Chem. Lett.* 2013, *4*, 999-1004.
53. Y. W. Chiu, M. H. Huang, *J. Phys. Chem. C* 2009, *113*, 6056-6060.
54. B. R. Taylor, S. M. Kauzlarich, *Chem. Mater.* 1999, *11*, 2493-2500.
55. A. M. Guloy, R. Ramlau, Z. Tang, W. Schnelle, M. Baitinger, Y. Grin, *Nature* 2006, *443*, 320-323.
56. S. Choi, J. Kim, N. S. Choi, M. G. Kim, S. Park, *ACS Nano* 2015, *9*, 2203-2212.
57. H. Jia, R. Kloepsch, X. He, J. P. Badillo, P. Gaom O. Fromm, T. Placke, M. Winter, *Chem. Mater.* 2014, *26*, 5683-5688.
58. K. H. Seng, M. Park, Z. P. Guo, H. K. Liu, J. Cho, *Nano Lett.* 2013, *13*, 1230-1236.
59. K. H. Seng, M. H. Park, Z. P. Guo, H. K. Liu, J. Cho, *Angew. Chem. Int. Ed.* 2012, *51*, 5657-5661.
60. T. Adachi, S. Sakka, *J. Non-Cryst. Solids*, 1988, *99*, 118-128.
61. T. D. Nguyen, W. Y. Hamad, M. J. MacLachlan, *Chem. Comm.* 2013, *49*, 11296-11298.
62. A. Kumar, Y. S. Negi, V. Choudhary, N. K. Bhardwaj, *J. Materials Physics Chemistry* 2014, *2*, 1-8.
63. H. P. Wu, J. F. Liu, M. Y. Ge, L. Niu, Y. W. Zeng, Y. W. Wang, G. L. Lv, L. N. Wang, G. Q. Zhang, J. Z. Jiang, *Chem. Mater.* 2006, *18*, 1817-1820.
64. X. . Wang, W. Q. Han, H. Chen, J. Bai, T. A. Tyson, X. Q. Yu, X. J. Wang, X. Q. Yang, *J. Am. Chem. Soc.* 2011, *133*, 20692-20695.
65. D. Wang, Y. L. Chang, Z. Liu, H. Dai, *J. Am. Chem. Soc.* 2005, *127*, 11871-11875.
66. E. J. Henderson, M. Seino, D. P. Puzzo, G. A. Ozin, *ACS Nano* 2010, *4*, 7683-7691.
67. K. E. Shopsowitz, A. Stahl, W. Y. Hamad, M. J. MacLachlan, *Angew. Chem. Int. Ed.* 2012, *51*, 6886-6890.
68. J. H. Jang, J. Koo, B. S. Bae, *J. Am. Ceram. Soc.* 2000, *83*, 1356-1360.
69. F. W. Yuan, H. J. Yang, H. Y. Tuan, *ACS Nano* 2012, *6*, 9932-9942.
70. D. Matioszek, W. S. Ojo, A. Cornejo, N. Katir, M. E. Ezzi, M. L. Troedec, H. Martinez, H. Gornitzka, A. Castel, C. Nayral, F. Delpech, *Dalton Trans.* 2015, *44*, 7242-7250.
71. Y. J. Cho, H. S. Im, H. S. Kim, Y. Myung, S. H. Back, Y. R. Lim, C. S. Jung, D. M. Jang, J. Park, E. H. Cha, W. Cho, F. Shojaei, H. S. Kang, *ACS Nano* 2013, *7*, 9075-9084.
72. Y. Xiao, M. Cao, *ACS Appl. Mater. Inter.* 2014, *6*, 12922-12930.
73. X. Gao, W. Luo, C. Zhong, D. Wexler, S. L. Chou, H. K. Liu, Z. Shi, G. Chen, K. Ozawa, J. Z. Wang, *Sci. Rep.* 2014, *4*, 6095.
74. J. Liu, K. Song, C. Zhu, C. C. Chen, P. A. Aken, J. Maier, Y. Yu, *ACS Nano* 2014, *8*, 7051-7059.
75. R. A. Huggins, *J. Power Sources* 1988, *22*, 341-350.
76. Robert M. Metzge, The Physical Chemist's Toolbox, *Wiley*, 2012, ISBN: 978-0-470-88925-1.

77. D. T. Ngo, R. S. Kalubarme, H. T. T. Le, C. N. Park, C. J. Park, *Nanoscale* 2015, *7*, 2552-2560.

Table of contents graphic: We have developed a new route for controlled co-assembly of a lyotropic liquid-crystalline phase of cellulose nanocrystals (CNCs) with a reactive precursor of germanium(IV) alkoxide in a mixed solvent system of water/DMF to produce tunable photonic chiral nematic GeO_2/CNC composites that were selectively pyrolyzed to recover freestanding films of amorphous GeO_2 and semiconducting mesoporous GeO_2/C and Ge/C replicas with chiral nematic organization.